Remote Sensing of Environment 112 (2008) 2886–2897

Contents lists available at ScienceDirect

Remote Sensing of Environment

journal homepage: www.elsevier.com/locate/rse

Temporal and spatial variability in biomass burned areas across the USA derived from the GOES fire product

Xiaoyang Zhang [a,*], Shobha Kondragunta [b]

[a] Earth Resources Technology, Inc at NOAA/NESDIS/Center for Satellite Applications and Research, Camp Springs, Maryland, USA
[b] NOAA/NESDIS/Center for Satellite Applications and Research, Camp Springs, Maryland, USA

ARTICLE INFO

Article history:
Received 11 September 2007
Received in revised form 9 January 2008
Accepted 7 February 2008

Keywords:
Burned area
Diurnal pattern
Temporal and spatial variability
GOES fire product

ABSTRACT

Burned area is a critical input to the algorithms of biomass burning emissions and understanding variability in fire activity due to climate change but it is difficult to estimate. This study presents a robust algorithm to reconstruct the patterns in burned areas across Contiguous United States (CONUS) in diurnal, seasonal, and interannual scales from 2000–2006. Specifically, burned areas in individual fire pixels are empirically calculated using diurnal variations in instantaneous fire sizes from the Geostationary Operational Environmental Satellites (GOES) WF_ABBA (Wildfire Automated Biomass Burning Algorithm) fire product. GOES burned areas exhibit diurnal variability with a temporal scale of half hours. The cumulative burned area during 9:00–16:00 local solar time accounts for 65%–81% of the total daily burned area. The diurnal variability is strongest in croplands compared to shrublands, grasslands, savannas, and forests. Analysis on a seasonal scale indicates that over 56% of burning occurs during summer (June–August). On average, the total annual burned area during the last seven years is $2.12\times10^4\pm0.41\times10^4$ km^2. The algorithm developed in this study can be applied to obtain burned area from the detections of GOES active fires at near real time, which can greatly improve the estimates of biomass burning emissions needed for predicting air quality.

1. Introduction

Wildland fires release a large amount of greenhouse gases and aerosols into the atmosphere. These emissions have significant impact on the global carbon cycle and air quality. As a result, a large number of efforts have focused on the estimates of biomass burning emissions on regional and global scales using *in situ* and satellite data (e.g., Duncan et al., 2003; Ito & Penner, 2004; Lü et al., 2006; Soja et al., 2004; WRAP, 2005a; Wiedinmyer et al., 2006). Currently, these emission estimates are highly uncertain (±50%) due to uncertainties in input parameters including burned area (Andreae & Merlet, 2001; Boschetti et al., 2004; French et al., 2004; Ichoku & Kaufman, 2005; Kasischke et al., 2003).

Several methods have been used to measure burned areas. For historical analyses, the burned areas from wildland fires are statistically derived from the characteristics of potential natural vegetation and ecological fire regimes (Leenhouts, 1998), and from local and national fire services or agencies (EPA, 2003; Lü et al., 2006). More recently, satellite data have been used to detect burned areas at regional scales (e.g., Fraser & Li, 2002; Pu et al., 2007; Zhang et al., 2003) and global scales, such as GLOBSCAR from ATSR (Simon et al., 2004), GBA2000 from SPOT VEGETATION (Tansey et al., 2004), and the MODIS burn scar product (Roy et al., 2002). Currently, burned areas retrieved from satellite data are generally available for a specific year at regional or global scales although MODIS burn scar product will produce continuous data in near future (Roy et al., 2002) and SPOT VEGETATION-based burned areas from 2000–2007 have been generated (http://www-tem.jrc.it/Disturbance_by_fire/products/burnt_areas/GlobalBurntAreas2000-2007.htm). In contrast, satellite-based active fire (hotspot) counts from various satellites provide fire occurrences in near real time and are available for multiple years (Justice et al., 2002; Prins et al., 1998). These fire count-covered areas are used to be a proxy of burned area for the calculation of biomass burning (e.g., Duncan et al., 2003; Eva & Lambin, 1998; Wiedinmyer et al., 2006). However, the fire count-covered areas generally overestimate actual burned areas because satellite sensors can usually detect fire occurrences in much smaller size (<100 m^2) than the pixel in the moderate and coarse resolution data (Giglio et al., 2003). On the other hand, both the limited instantaneous observations within a day (twice from AVHRR-18, once from AVHRR-17, and four times from Terra plus Aqua MODIS) and cloud cover often result in missing detections of temporal fire events. Therefore, these fire counts generally capture the majority of large fire events but the corresponding burned area estimated is of considerable uncertainty (Giglio et al., 2003; Li et al., 2000). Recent studies show that the burned areas derived from various methods (field inventory, satellite-based burn scars, and satellite hotspots) differ from 3 to 10 times in Siberia (Conard et al., 2002), about two orders of magnitude in global coverage, and 7 times in North America (Boschetti et al., 2004).

A number of methods have been developed to improve the estimates of burned areas from satellite-based active fire observations

* Corresponding author.
E-mail address: xiaoyang.zhang@noaa.gov (X. Zhang).

0034-4257/$ – see front matter © 2008 Elsevier Inc. All rights reserved.
doi:10.1016/j.rse.2008.02.006

(Giglio et al., 2006; Kasischke et al., 2003; Pereira et al., 1999; Scholes et al., 1996). Burned areas are linearly correlated to fire counts from AVHRR, ARSR, and MODIS data over a large spatial grid (0.5°–1°) on a monthly scale (Kasischke et al., 2003; Pereira et al., 1999; Scholes et al., 1996). A more sophisticated method, which uses the varied proportion between burned areas and fire counts and a regression tree algorithm, is used to estimate global burned area at a 1° spatial resolution from MODIS active fire counts (Giglio et al., 2006). Certainly, the resultant burned areas are to some extent improved, but the accuracy in these estimates still varies greatly with different regions (e.g. Eva & Lambin, 1998; Giglio et al., 2006; Kasischke et al., 2003; Pereira et al., 1999).

Unlike other satellites, National Oceanic and Atmospheric Administration (NOAA's) Geostationary Operational Environmental Satellite (GOES) provides high temporal frequency of active fire observations. From the GOES data, Wildfire Automated Biomass Burning Algorithm (WF_ABBA) detects subpixel fire sizes every half hour (Prins & Menzel, 1994; Prins et al., 1998). The GOES fire dataset has been demonstrated to be a potentially powerful tool in estimating smoke aerosol emissions in near real time for Naval Research Laboratory (NRL) aerosol forecasts (Prins et al., 1998; Reid et al., 2004). However, to estimate the variation in biomass burning emissions accurately, the challenge is to minimize the effects of missed observations of instantaneous fire sizes and to convert subpixel fire sizes to burned areas. To this end, this study examines diurnal variability of GOES instantaneous subpixel fire sizes for a variety of ecosystems across Contiguous United States (CONUS) and fits the diurnal pattern in fire sizes using a Fourier function. The fitted model is then applied to empirically simulate burned areas in each fire event detected from GOES satellite. The simulated burned areas are evaluated and validated using the burn scars detected from post-fire Landsat ETM+ (Enhanced Thematic Mapper plus) imagery and national inventory fire data across CONUS. We further investigate the spatial and temporal patterns in burned areas at diurnal, seasonal, and interannual scales from 2000 to 2006.

2. Data

2.1. Instantaneous fire size in GOES WF_ABBA product

The WF_ABBA derives fire products from the GOES imager every half hour (Prins & Menzel, 1992; Prins et al., 1998; Weaver et al., 2004). This algorithm applies Dozier's (1981) bi-spectral method to detect instantaneous fire sizes in subpixels using 3.9 μm and 10.7 μm infrared bands after locating and characterizing hotspot pixels with a nadir spatial resolution of 4 km (Prins & Menzel, 1994). This product contains the time of fire detection, fire location in latitude and longitude, instantaneous subpixel fire size, corresponding ecosystem type, and quality flag (from 0 to 5). The ecosystem type in the fire product is based on USGS (US Geological Survey) Global Land Cover Characterization (GLCC) dataset (Brown et al., 1999). The quality flag represents the confidence of fire detections with six different levels that indicate a fire pixel being processed (flag 0 — subpixel instantaneous estimation of fire size and temperature), saturated (flag 1 — saturated fire pixel), cloud-contaminated (flag 2 — cloud-contaminated fire pixel), high probability (flag 3 — high probability fire pixel), medium probability (flag 4 — medium probability fire pixel), and low probability (flag 5 — low probability fire pixel). To minimize false fires caused by cloud edges, extreme solar zenith angles, and sensor noise related to uncertainty in radiance detection, interchannel spatial misregistration, geo-location, and Point Response Function (Cahoon et al., 2000; Giglio & Kendall, 2001; Robinson, 1991), the WF_ABBA uses a temporal filter to exclude the fire pixels that are only detected once within the past 12 h (Schmidt & Prins, 2003). In this study, we collect the GOES WF_ABBA fire data between January 2000 and December 2006 across CONUS. Note that these fire data are retrieved from GOES-8 and 12 using ABBA v5.9 for September 2000–March 2002 and ABBA v6.0 for other periods. ABBA v6.0 is expected to better discriminate false detections caused by cloud edge than ABBA v5.9, but these two versions produce very similar fire detections.

There are two major limitations in the fire data from GOES WF_ABBA. First, subpixel fire sizes are only calculated in about 38% of the instantaneous fire observations which are referred to as the processed fire pixels (flag 0) (Fig. 1). Among the rest of fire detections without fire size estimates, there is confidence in about half of the fire observations (flags 1–4) and about half that might be false detects (flag 5) (Fig. 1).

Second, observations of diurnal fires may, to a great extent, be obstructed by cloud cover and other factors. Clouds often prevent the sensor from seeing fires and reduce the amount of active fire observations (Giglio et al., 2003; Prins & Menzel, 1992; Roberts et al., 2005). Generally, the frequency of cloud occurrence in diurnal patterns is over 50% in both summer and winter across CONUS (Schreiner et al., 2001), which is partially responsible for the missed detections of fires, particularly in the observations of diurnal patterns. Furthermore, satellite detection of active fire is also impacted by heavy fire smokes, hot and reflective surfaces, and weakly emitting fire pixels (Roberts et al., 2005). For example, the Hayman fire in the Front Range of Central Colorado burned about 550 km^2 of area within the fire perimeter in June 2002, but the instantaneous fires were only continuously observed in DOY (day of year) 160.

2.2. Burned area

We acquire both high resolution Landsat ETM+ imagery and ground-based data to train and validate an algorithm that derives burned areas from GOES ABBA data. First, we obtain areas within fire perimeters and Landsat ETM+ imagery (30 m) from the Joint NPS

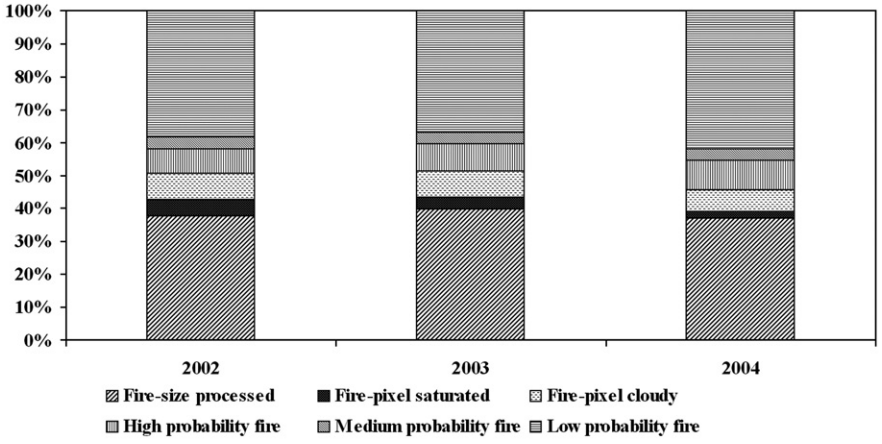

Fig. 1. Proportions of GOES fire observations in different quality levels over CONUS based on fire data from 2002–2005.

(National Park Service)-USGS National Burn Severity Mapping Project (http://burnseverity.cr.usgs.gov/fire_main.asp). This project also provides the dates of fire occurrences for the selected fire events. In this study, we collect burn scars from 20 fire events in 2002 (used for training algorithm to simulate GOES burned areas) and 14 fire events during 2003–2005 (used for validation) across CONUS, which are observed in different land cover types such as forests, savannas, shrublands, and grasslands. Because there is a certain amount of unburned islands within the fire perimeters, we calculate actual burn scars within the fire perimeters from ETM+ imagery using the Normalized Burn Ratio (NBR). The NBR is first computed as the difference between near-infrared and middle-infrared reflectance (Key, 2006; Key & Benson, 1999; Epting et al., 2005). It is then used to calculate the differenced Normalized Burn Ratio (dNBR) by comparing the pre- and post-fire NBR values. To improve the estimates of burned areas, we remove unburned islands within the fire perimeters of individual fire events using dNBR method. For the dataset used in this study, the unburned area within the fire perimeter is about 22.3%±15.1%, which is found to be independent of the size of burn scar (0.5–1452 km^2) and land ecosystems. If these unburned islands are not excluded, burned area can be overestimated. Note that ETM+ NBR is one of the best methods to estimate burned areas, but the accuracy may be affected by background soil color, re-sprouting from burned plants, blackening or scorching of trees, and time period of the pre- and post-fire ETM+ imagery (Roy et al., 2006; Van Wagtendonk et al., 2004). Additionally, burn scars caused by surface fires under dense tree canopy are hard to detect from ETM+ data.

The second dataset of burned area is obtained from Inter-Regional Program Office (RPO) 2002 National Wildfire Emission Inventory (NWEI) (WRAP, 2005a) for comparison with simulated GOES burned areas in 2002. We use all the NWEI burned area data that are obtained from fire reports of federal, state, and local agencies. Although this dataset provides the most accurate *in situ* burned areas available so far, there are some limitations. Generally, the burned area reported for a given fire event represents the total area within the fire's perimeter, which contains 24%±17% (4–54%) of the acreage without burning (WRAP, 2005b). Further, this dataset only provides one geo-location for a fire event instead of a spatial coverage, and the reported locations could be erroneous (WRAP, 2005a). Particularly, the latitude and longitude in many prescribed fires are not provided, so that the centroid coordinates of the county shape are written in the activity records. Moreover, a number of small fires were not reported. However, GOES imager is geostationary and is able to detect many of the fires that are reported in the NWEI (even though reported at county centroids or too small a wildfire to report or non-reported agricultural burning). Even though there are limitations in NWEI burned areas, these data covering all CONUS are very useful for comparing and validating the burned areas calculated from GOES fire data in 2002.

3. Method

Because the burned area is generally proportional to active fire pixel counts (Giglio et al., 2006; Kasischke et al., 2003; Pereira et al., 1999), instantaneous fire size detected by GOES imager is assumed to be a proxy for burned area. Specifically, the area burned is in this context considered as a function of subpixel fire sizes detected from GOES WF_ABBA and is simply described as:

$$A = \alpha F \tag{1}$$

where A is the area burned within a specified time period (km^2), F is the subpixel fire size (km^2), and α is a coefficient of conversion.

To calculate the burned areas using Eq. (1), the fire size and coefficient α are determined as described in the following two sections.

3.1. Determining representatives of diurnal fire sizes

To reconstruct missed fire sizes, we establish representatives of diurnal fire sizes by examining the GOES WF_ABBA fire product. Diurnal variation in fire intensity has been used for wildland fire management (Beck et al., 2001; Finn, 2001) and widely observed from various satellite data (Giglio, 2007; Justice et al., 2002; Roberts et al., 2005). The basic diurnal pattern exhibits high fire intensity during daytime with a peak at noon or afternoon while fire is weak during night. This pattern is strongly associated with diurnal variations in fire weather conditions (Schroeder & Buck, 1970), fuel moisture (Rothermel & Mutch, 1986) and fuel temperature (Countryman, 1966). In this study, we select all half-hourly subpixel fire sizes from GOES fire data (flag 0) between 2002 and 2005, and stratify them based on ecosystems. The ecosystems are classified from GLCC ecosystem types into forests, savannas, shrublands, grasslands, and croplands. For each ecosystem, the fire sizes in a given half hour are averaged to generate a diurnal variation. This averaging can reveal the temporal pattern of variation although the absolute values may vary for individual fire pixels. The corresponding coordinated universal time (UTC) of fire occurrence is converted to local solar time (LST).

The averaged fire sizes are fitted using a Fourier model to create a set of representative curves of diurnal patterns for forests, savannas, shrublands, grasslands, and croplands, respectively. Because the subpixel fire size may contain uncertainties caused by background radiance determination, atmospheric radiance correction, and fire properties

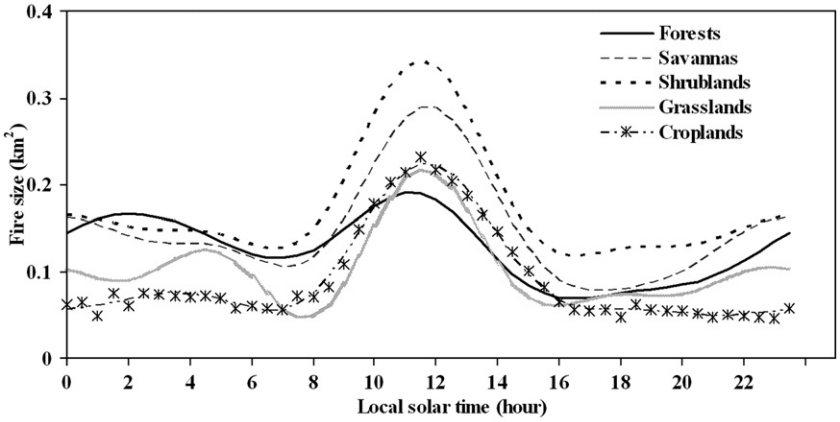

Fig. 2. Diurnal fire sizes (average data from 2002–2005) fitted using the DFT model for various ecosystems. The asterisks indicate the examples of original data points of fire sizes in croplands, but original data for other ecosystems are not presented here.

(Giglio & Kendall, 2001; Prins & Menzel, 1994), a suitable curve fitting should smooth the impact of uncertainties in fire detections without affecting the fire size behaviors and should fill the missed fire sizes (such as GOES fire flags 1–5 and instantaneous fire undetected in GOES fire product). Therefore, we fit the diurnal fire sizes using the Discrete Fourier Transform (DFT) which is decomposed into a set of trigonometric forms in the following equation (Briggs & Hensen, 1995):

$$F_{(t)} = a_0 + a_1 \cos\left(\frac{2\pi t}{N}\right) + b_1 \sin\left(\frac{2\pi t}{N}\right) + a_2 \cos\left(\frac{4\pi t}{N}\right) + b_2 \sin\left(\frac{4\pi t}{N}\right) + \ldots + a_k \cos\left(\frac{2k\pi t}{N}\right) + b_k \sin\left(\frac{2k\pi t}{N}\right) \quad (2)$$

where $F_{(t)}$ is half-hourly fire size (km^2) at time t (hour), N is the number of samples in the time series, a_0 is the mean, a_1 and b_1 are first-order trigonometric, a_2 and b_2 are second-order trigonometric, and so on to k_{th} order.

The diurnal fire size is well fitted using 4 harmonics of DFT formula (Fig. 2). The standard deviation between the original data and the fitted curve is 0.0078, 0.0095, 0.0112, 0.03125, and 0.005 km^2 for forests, savannas, shrubs, grasses, and crops in turn. These values are much smaller than the diurnal fire sizes, which indicate that the curve fitting works reasonably well. The error of the curve fitting is largest in grasslands where the samples of half-hourly fire sizes are relatively scattered.

Fire size fitted from GEOS subpixel fire data in various ecosystems presents a similar diurnal pattern, which is largest around 13:00 LST (Fig. 2). The half-hourly fire size in shrublands and savannas is generally larger than 0.2 km^2 during 10:00–15:00 LST while it varies between 0.1 and 0.2 km^2 during other hours. The diurnal pattern is most distinctive in croplands where large fire size dominates in 9:00–17:00 LST while the value is only about 0.05 km^2 in other time periods. In contrast, the diurnal fire size in forests is relatively stable throughout a day, which varies slightly around 0.15 km^2. These fire sizes are within the reasonable region of GOES ABBA product (Prins et al., 1998).

3.2. Simulating a diurnal curve for an individual fire pixel

Before generating a diurnal curve for a specified fire pixel, geo-location errors in GOES fire pixels are reduced. Generally, wildfires burn for several hours extending the fire from a small area in a GOES pixel to eventually covering the whole pixel (~4 km) because fire spread rate is about 0.06–0.21 km/h (Loboda & Csiszar, 2007; McRae et al., 2005). Geo-location shift in GOES instantaneous observations may place the fire in a nearby GOES pixel. To reduce the geo-location error, we cluster fire observations based on the following criteria. (1) If fire observations in any two neighbor pixels (a 0.08° buffer, about 10 km) are temporally coincident at any instantaneous observations within a day, these are treated as separate fire pixels. If they are not observed at the same time at all within one day, they might belong to the same fire pixel. Thus they are clustered temporally. Note that this assumption may not be applicable for very small fires lasting less than a half hour because GOES imager detects fire every half hour. (2) The pixel with fewer temporal fire observations is clustered to the pixel with more temporal observations.

The diurnal curve of fire sizes for a given fire pixel is then generated by adjusting the corresponding representative diurnal curve. This processing assumes that the shape of the diurnal curve for a given pixel in the same ecosystem is similar. Thus, only the shape of the representative curve is imposed on the detected fire sizes in the given pixel by adding an offset.

$$\mathrm{Fs}_{(i,j,p,t)} = F_{(p,t)} + D_{(i,j,p)} \quad (3)$$

where Fs represents the simulated fire size, F is the representative diurnal fire sizes from Eq. (2), D is a offset, i and j indicate the location of the fire pixel, p is the ecosystem type in the related pixel, and t is time in a half hour.

The offset is calculated from the detected GOES fire sizes in a pixel and the representative curve of the related ecosystem. Specifically, the offset D is calculated using least square method from the available fire sizes (flag 0) for a fire pixel and the related values from a representative curve (Fig. 3). For the fire pixels where the number of the processed instantaneous fire sizes is less than three, the offset is assumed to be zero.

3.3. Calculating the optimal threshold of fire duration and the conversion coefficient of burned area

The fire duration in a day is determined for each fire pixel. In a fire event, large forest fires usually last for several days while some prescribed fires are small and only last for several hours or less. However, fire duration is difficult to determine directly from GOES WF_ABBA fire data accurately because of the gaps associated to the interferences from cloud cover, smokes, weak fire emitting, and other observation factors. Thus, the following criteria are applied for this purpose. (1) The fire pixel is considered a false detect if all the temporal fire observations are only with low probability (flag 5) and less than three times within a day. (2) The fire occurrences between the first and last observations (flags 0–5) are assumed to be continuous because the GOES fire pixels are very coarse (~4 km). (3) Fires might exist beyond the time period between the first and last GOES detections. For

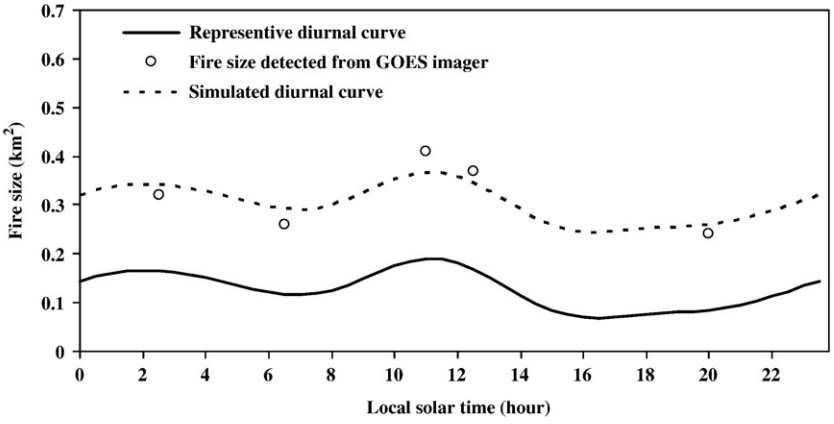

Fig. 3. Simulating the diurnal pattern of fire sizes from available fire sizes observed in a pixel (as an example) located in Hayman fire and the representative diurnal curve in forest ecosystem.

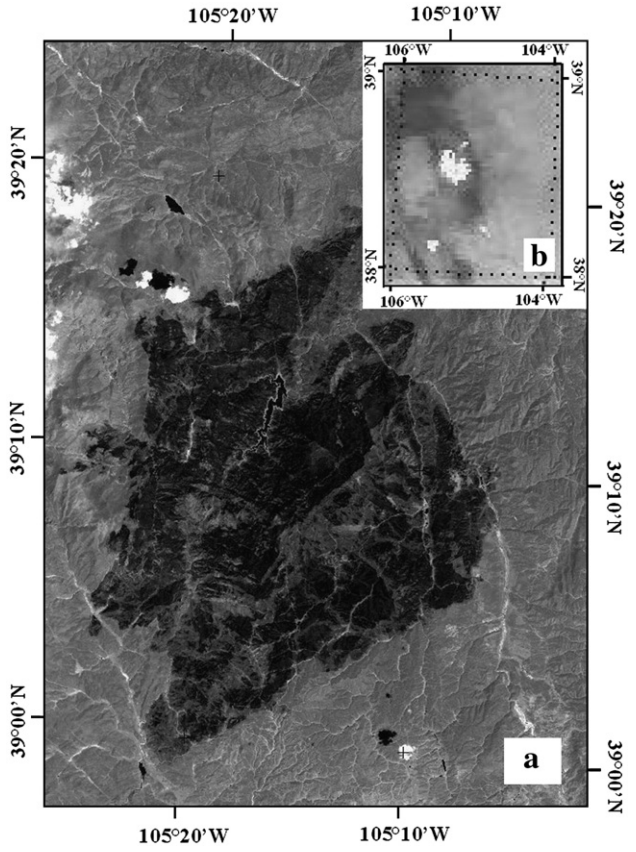

Fig. 4. Hayman fire event (as an example) in June 2002 observed from ETM+ and GOES imager. (a) Burn scar (black color) in ETM+ band 4 (30 m); and (b) hotspots (white color) in GOES imager band 2 (~4 km). Note that subpixel fire size in a GOES hotspot could be very small.

example, GOES imager may delay the detection of fire occurrence because of the lag that a darkened pixel becomes visually evident (Weaver et al., 2004). Thus, fires in a pixel are assumed to last for whole the day if the confident fire observations (flags 0–4) are more than four times around the middle in the local time and observed fire duration (flags 0–5) is longer than a certain threshold (see the following two paragraphs). (4) If fire duration is less than the threshold, it is assumed to be the period between the first and last GOES observations. (5) The half-hourly fire size is assumed to proportionally represent burned area as described in Eq. (1) and the cumulative burned areas within a pixel should be no larger than the GOES pixel size. Criteria 1 and 2 are determined straightforward based on WF_ABBA fire data. Nevertheless, the threshold of fire duration in criterion 3 and the proportional coefficient α in criterion 5 are complex and statistically determined as described in the following paragraph.

To calculate the optimal threshold of fire duration to determine whether the fire within a pixel could last for a day, we compare the cumulative GOES fire sizes simulated using diurnal representative curves with the 20 burn scars detected from ETM+ imagery in 2002 (ETM+-based burn scars in 2003–2005 are used for validation). Specifically, we conduct a set of comparisons with different thresholds that are set from 1 to 24 h with 1 h interval. According to a given threshold and 4 criteria described in the above paragraph, we calculate all the GOES fire sizes from active fire hotspots during the time period and spatial coverage in a fire event, which are corresponded to the specified ETM+ burn scar (Fig. 4). Thus, we obtain total GOES fire sizes in a fire event and compare them with whole area of ETM+ burn scar. We then statistically compute a set of α values and root mean square error (RMSE) between cumulative fire sizes and ETM+ burn scars using a linear regression method. In this process, parameters A and F in Eq. (1) are substituted using the ETM+-based burn scar and the GOES cumulative fire size for each fire event, separately. The optimal α and threshold of fire duration are obtained when RMSE reaches minimum and α reaches a constant.

Comparison reveals that RMSE between cumulative GOES fire sizes and ETM+ burn scars in 2002 decreases while coefficient α increases with the increase of the threshold of fire duration (Fig. 5). Particularly, RMSE reaches minimum if the duration threshold is set to 9–14 h. Correspondingly, α is 1.002 for the time duration threshold ranging from 11–14 h. The simulated half-hourly fire size is equivalent to burned area under these conditions. In other words, this result suggests that the daily burned area could be simulated by cumulating the fire size in whole the diurnal curve if fire duration is longer than 14 h otherwise it is only cumulated from the diurnal period between the first and last fire observations. Note that the estimates of burned areas do not significantly improve if the threshold of fire duration is lengthened.

Based on above optimal values of fire duration and conversion coefficient, the simulated GOES burned areas match the ETM+-based burn scars very well (Fig. 6). The samples are distributed closely along a 1:1 line with a correlation slope of 0.92 and R^2 of 0.99. In contrast, the cumulative fire size from the original GOES fire data (without curve fitting) only accounts for about 21.5% of the total burned areas. Evidently, the diurnal curve of the simulated fire size greatly improves the estimates of burned areas.

Using the optimal α and fire-duration threshold, we estimate burned area for each fire pixel from GOES fire product in 2000–2006. Then, we investigate the variations in burned areas at various temporal and spatial patterns across CONUS.

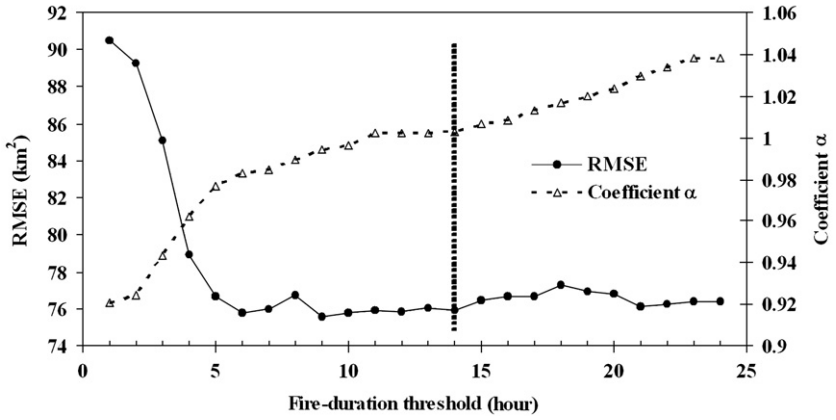

Fig. 5. Variation in the RMSE and conversion coefficient α between ETM+ burn scars in 2002 and cumulative GOES fire sizes with the increase of GOES fire-duration threshold.

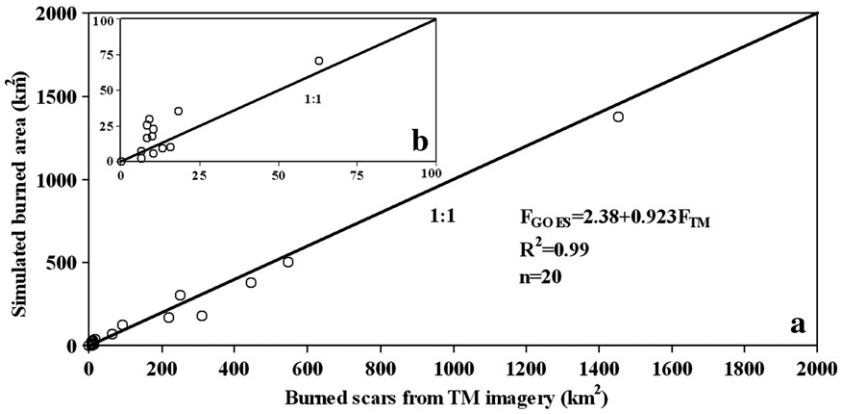

Fig. 6. Comparison between the simulated GOES burned areas and ETM+-based burn scars in 2002 (a). The details of burned areas for the small fire events are displayed in (b).

3.4. Evaluating the simulated GOES burned area

The burned areas simulated from GOES diurnal fire sizes are validated using two independent datasets. The simulated burned areas are first compared with the burn scars detected from ETM+ imagery from 2003–2005. This verifies the capability of GOES fire sizes for the estimates of burned areas for individual fire events.

The simulated GOES burned areas in 2002 are further compared to the burned areas from NWEI in 2002 across CONUS. Because NWEI only provided a point location with latitude and longitude rather than a spatial coverage for a fire event, it is hard to match each fire event between GOES observations and NWEI data. Therefore, the burned areas are divided into grid cells with a spatial resolution of 0.33° (20 min) across CONUS to minimize the discrepancy. Furthermore, we also compare the data in coarser resolution of 0.5° (30 min) and 1°, which are generally used in atmospheric circular models. This allows the estimates of variance of burned areas at different scales for environmental modeling and reduces spatial geo-location errors (Boschetti et al., 2006).

4. Results

4.1. Evaluation of algorithm

Evaluations using two independent datasets show that the developed algorithm is robust in simulating burned areas. The area simulated from GOES fire sizes matches well with burn scars derived from

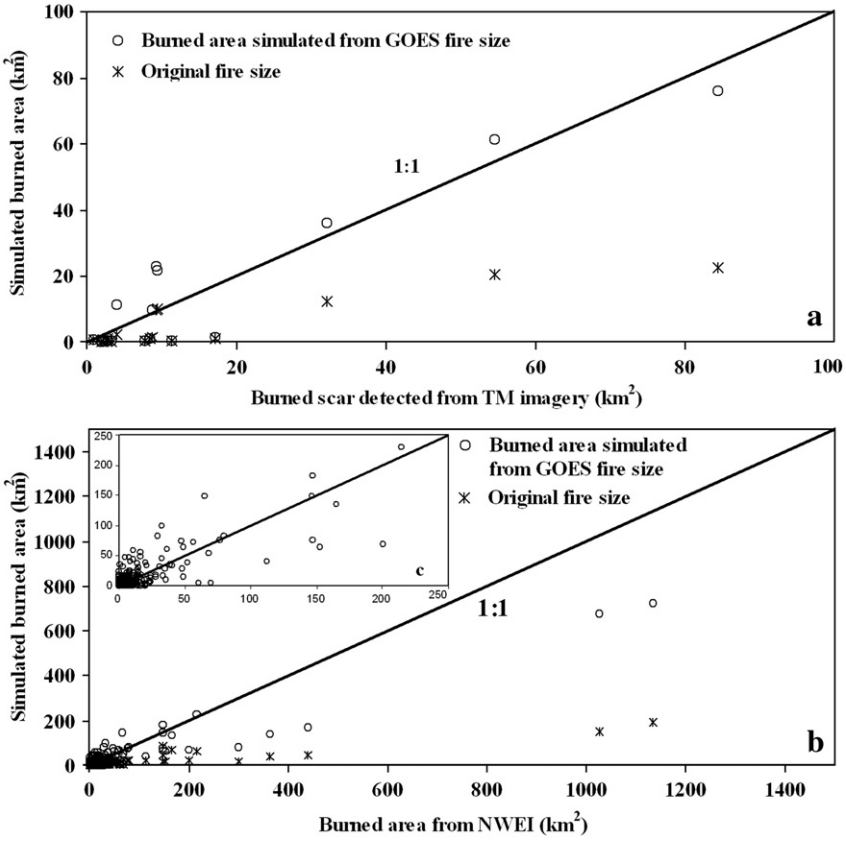

Fig. 7. Comparison of the simulated GOES burned areas with the burn scars detected from ETM+ imagery in 2003–2005(a) and the national inventory data in the grids of 20 min in 2002 (b). The details for the grids with small values of burned areas are displayed in (c). Original fire size indicates the GOES fire size without fitting using diurnal patterns.

ETM+ imagery during 2003–2005 (Fig. 7a). Particularly, the simulated burned area is very close to ETM+ burn scar in large fire events. However, the simulated burned area is relatively poor in some small fire events that fires are only detected once in the diurnal pattern or no instantaneous fire sizes are provided in GOES fire product (flags are 1–5 for all GOES fire detections). Overall, the simulated GOES burned areas are significantly correlated with ETM+ burn scars (R^2=0.82) and without significant bias (slope=0.99) (Fig. 7a). This suggests that the burned area simulated from GOES fire data is a good proxy of burn scar in a large fire event. It is important to note that more than 80% of the burned area is caused by large fires (>20 km^2) which are more important for biomass burning emissions and land cover change (Giglio et al., 2006; Soja et al., 2007).

The simulated GOES burned area also compares well to the burned area in NWEI data across CONUS (Fig. 7b). The data pairs reveal that the simulated GOES burned area accounts for 91%, 91%, and 70% of the variation in burned areas from NWEI when the resolution of the matched grid cell is 0.33°, 0.5°, and 1°, respectively. Correspondingly, the linear regression slope (NWEI data as independent variable) is 0.62, 0.66 and 0.78. The analysis of the total values in the matched

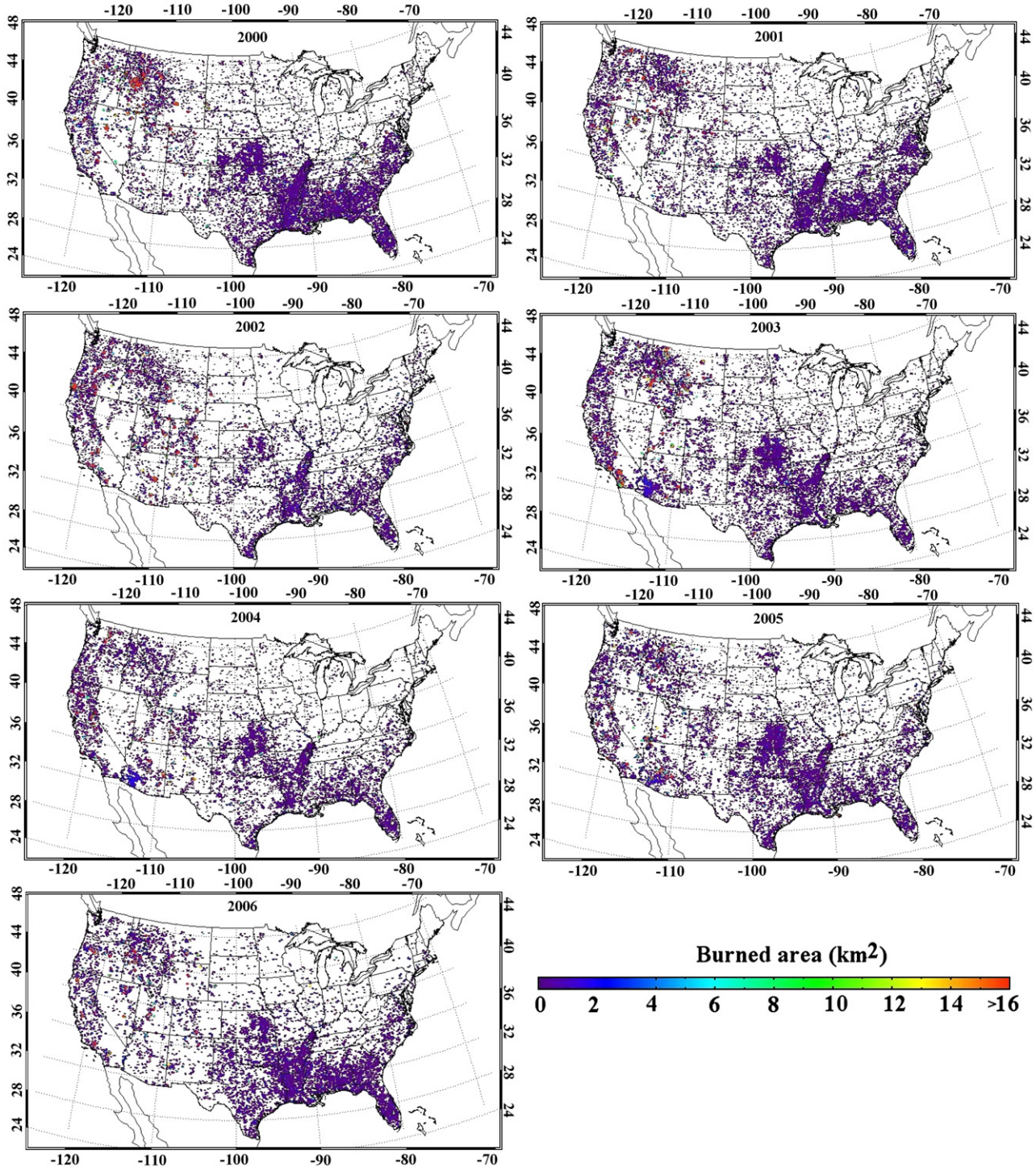

Fig. 8. Spatial patterns in burned areas (km^2) in GOES fire pixels from 2000 to 2006. Note that the size of the dots increases slightly for large burned areas for the display purpose.

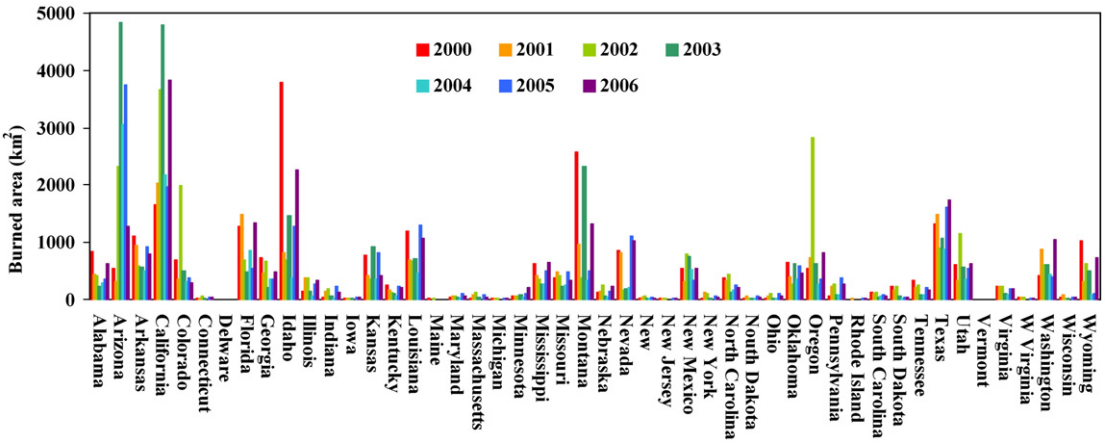

Fig. 9. Variations in burned areas for different states across CONUS.

grids indicates that the simulated GOES burned area is 15% smaller than that from NWEI. The large burned areas are smaller in simulated GOES data than those in NWEI. This result suggests that the simulated GOES burned area is reasonable because NWEI data include a certain amount of non-burned areas in fire perimeters. In contrast, if the GOES fire data are not simulated using diurnal patterns, the cumulated fire sizes in these matched grids are only about 26% of the NWEI burned areas.

4.2. Spatial pattern in burned areas across CONUS

Fig. 8 presents spatial distributions of annual burned areas over CONUS from 2000 to 2006. The burned areas reflect that fires generally occur in the western US, southeastern US, and along central and southern Mississippi Valley, while fire occurrences are limited in northeastern and southwestern regions. This spatial pattern is likely associated with climate, ecosystem, and human activity. Because of the relatively dry climate and dense forests (or shrubs) in the western US (Schoennagel et al., 2004), burned areas in many individual fire events could be larger than several GOES pixels. Relatively, burned areas are small in individual fire events but fire occurrences are highly frequent and densely distributed along central and southern Mississippi Valley, which is typically related to agriculture activities. Over CONUS, the frequency of fire pixels for the seven years is 81.9±2.5%, 14.2±2.0%, 2.3±0.5%, and 1.5±0.6% for the burned areas being <1 km^2, 1–5 km^2, 5–10 km^2, and >10 km^2, respectively.

Burned areas are distinctively different at state levels (Fig. 9). Generally, burned areas are large in California and Arizona for all these years, and Idaho, Montana, Oregon, Colorado, Florida, and Texas in some individual years. Annual burned area could be over 3500 km^2 in California, Arizona, and Idaho. On average during the seven years, the top ten states with large annual burned area (650–2900 km^2) in ascending order are Colorado, Arkansas, Louisiana, Oregon, Florida, Montana, Texas, Idaho, Arizona, and California, in turn. Certainly, biomass burning contributes significantly to the air quality in these states and results in high incidences of poor air quality. Further, the difference in burned areas will help air quality community to determine the states with possible poor air quality caused by fires.

4.3. Temporal variability in burned areas

Diurnal pattern in the burned area simulated from GOES fire data reveals that fires mainly occur during 9:00–16:00 LST across CONUS (Fig. 10). The corresponding proportion of the burned area is 64.8%, 74.0%, 67.6%, 76.1%, 80.5%, 81.2%, and 74.1% from 2000–2006, respectively. The burned area is larger than 14%/h during 11:00–14:00 LST where the peaks appear in the diurnal cycles. By contrast, the hourly value is less than 3% from 17:00 to next 9:00 LST. The strong diurnal pattern is consistent in all these years regardless of the variation in total burned area. These resultant diurnal cycles are similar to the diurnal fire growth and fuel consumption for air quality modeling (WRAP, 2005a), the strong diurnal variability in biomass burning that

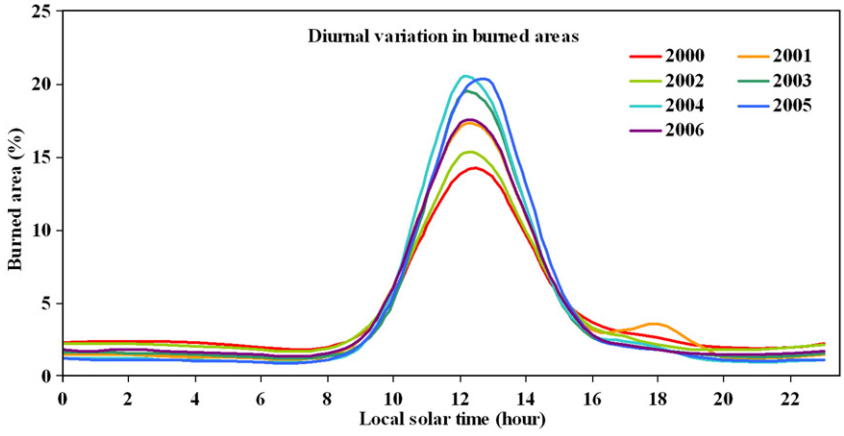

Fig. 10. Diurnal patterns in the simulated burned areas (%/h).

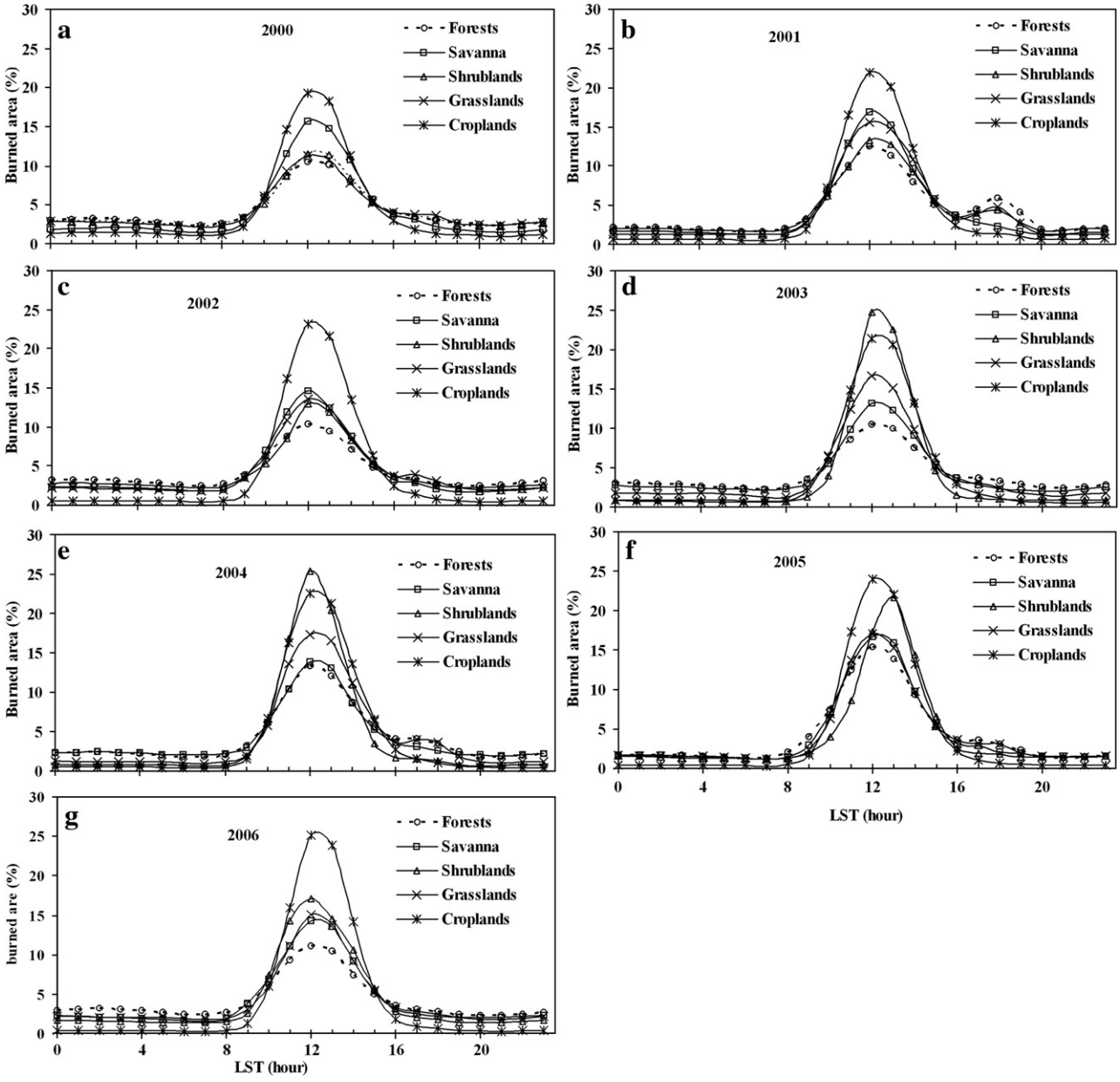

Fig. 11. Diurnal variability in the simulated burned areas varying with ecosystems.

is derived from TRMM (Tropical Rainfall Measuring Mission) fire pixel counts (Giglio, 2007; Justice et al., 2002), and the SEVIRI (Spinning Enhanced Visible and Infrared Imager) fire radiative power (Roberts et al., 2005). This kind of fire activity is subject to both human activities and meteorological conditions (Malingreau, 1990). In herbaceous vegetation region, fuels are finer and relatively dry quickly, so the diurnal fire cycle is dictated primarily by human activity (Giglio, 2007). In forest region, fuel moisture and humidity (ambient humidity) play a significant role in the diurnal pattern (Beck et al., 2001; Cochrane, 2003; Giglio, 2007). Note that the possible diurnal variations in the factors (such as clouds) that affect the GOES fire detections may cause a bias in the diurnal pattern in the simulated burned areas.

Diurnal cycles of burned areas vary with ecosystem types (Fig. 11). Although the peak of the diurnal cycle occurs consistently for various ecosystems except for the shrublands in 2005, the areas burned during peak fire activities (10:00–15:00 LST) account for 52.1%, 61.8%, 66.9%, 62.5%, and 84.9% of daily total areas in forests, savannas, shrublands, grasslands, and croplands, respectively. During off-peak time periods, the hourly burned areas are less than 4% in all these ecosystems. Specifically, they are very limited (<0.5%/h) in croplands because agricultural fires are strongly controlled by human activities during daytime. In contrast, the burned areas in forests are relatively high with a proportion of about 2–4%/h during off-peak time, because forest fires often burn for several days. The proportion of burned area in other ecosystems varies between those in croplands and forests. These results demonstrate that the peak time in the areas of biomass burning is similar for these ecosystems.

Burned area exhibits a distinctive seasonality (Fig. 12). The largest monthly burned area could be over 6×10^3 km^2 in 2000, 2002, 2003 and 2006 while it is less than 4×10^3 km^2 in 2001 and 2004. In contrast, the minimum monthly burned area is less than 160 km^2 during these years, where the smallest value is 71 km^2 in December 2002. The seasonal peak of biomass burning generally occurs during June–August, which is supported by AVHRR-based burned areas (Pu et al., 2007). The relative burned area during summer (June–August) is 70.9%, 55.9%, 78.1%, 68.2%, 64.2%, 67.6%, and 65.3% from 2000 to 2006, respectively. The seasonal

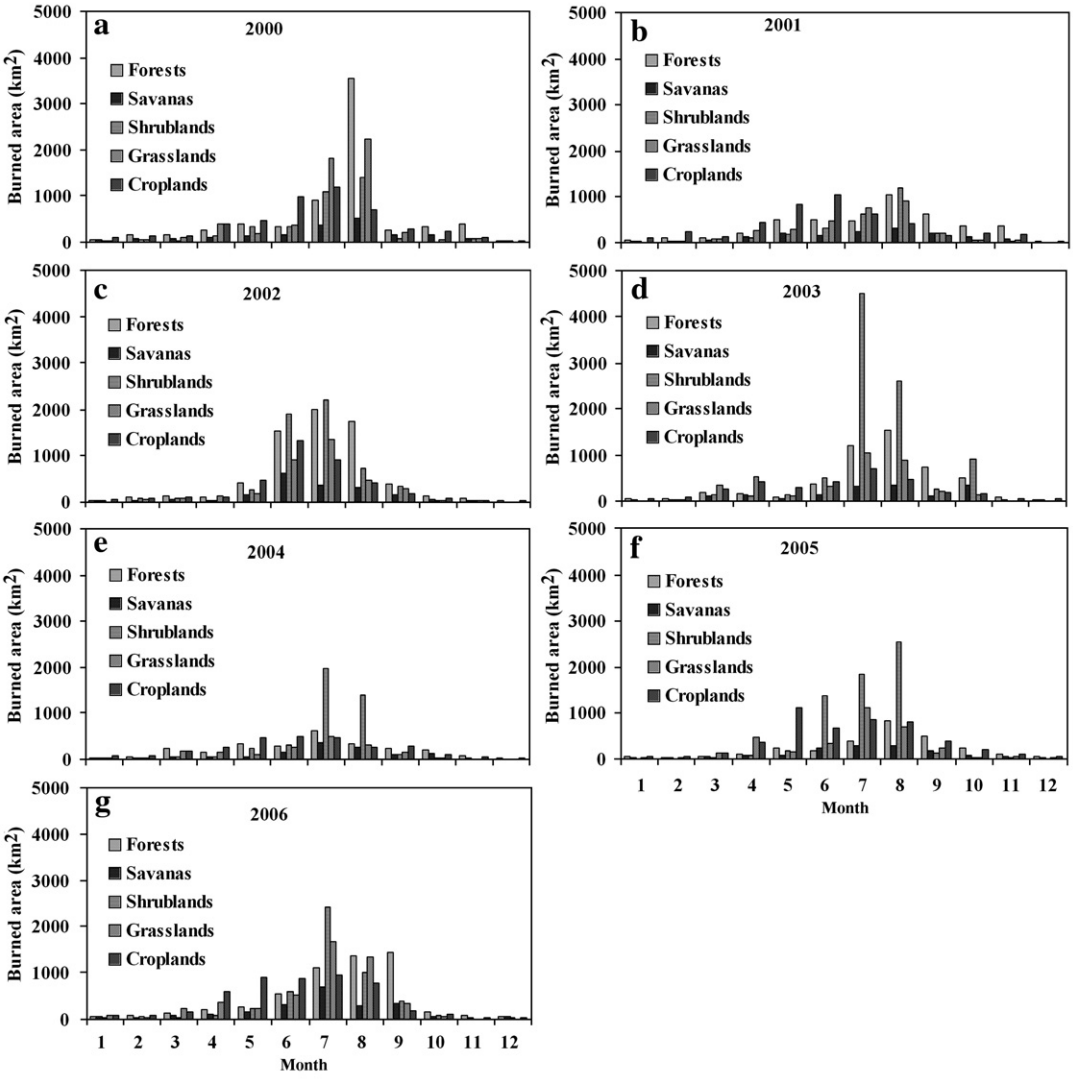

Fig. 12. Seasonal variations in the simulated burned areas. a–g represent the monthly burned areas for different ecosystems from 2000–2006, separately.

variability is strongest in shrublands and grasslands where the burned areas in summer are over 76% and 62%, separately, for all the individual years. However, the burned areas reflect that large fires may occasionally occur in other individual months, such as October in 2001 and 2003 and September in 2006. In contrast, the seasonality is relatively weaker in croplands, where the burned areas are large from April to September. This pattern reflects that agricultural fires could be set during the harvesting, post-harvesting, and pre-planting periods across CONUS. It is due to the fact that the agricultural burning is used for clearing crop residue, fertilizing the soil, and eliminating insects and disease from the fields (Chidumayo, 1987; Korontzi et al., 2006).

Interannual variation in burned area is significant. The burned area is 2.44×10^4, 1.80×10^4, 2.38×10^4, 2.37×10^4, 1.36×10^4, 2.10×10^4, and 2.42×10^4 km^2 from 2000 to 2006, in turn, which is largest in 2000

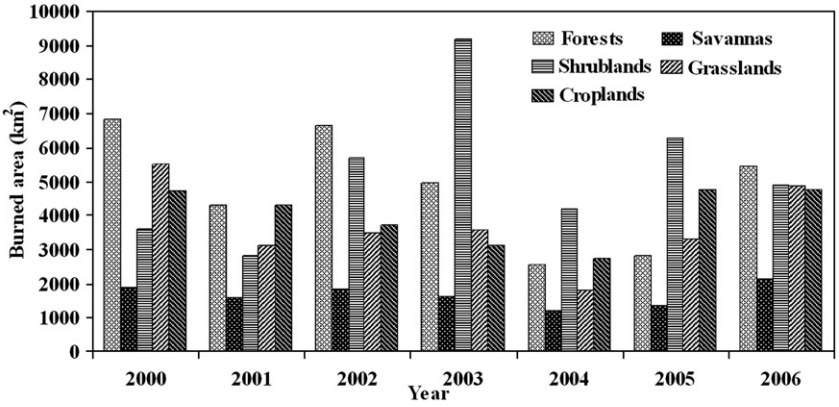

Fig. 13. Interannual variations in the simulated burned areas for different ecosystems.

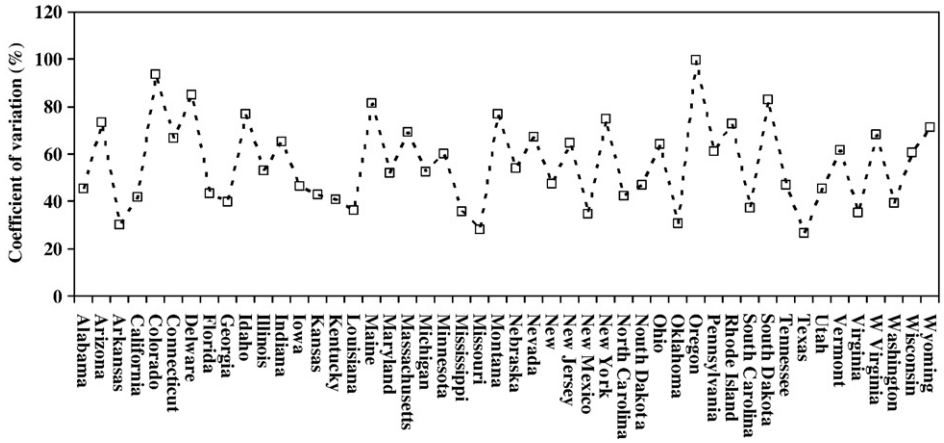

Fig. 14. Interannual variations (coefficient of variation) in burned areas for different states from 2000–2006.

while smallest in 2004. The total annual burned area experiences no significant temporal trends and the average is $2.12\times10^4\pm0.41\times10^4$ km^2. At ecosystem levels, the burned area decreases with a rate of 406 and 117 km^2/year for forests and grasslands, increases with 334 km^2/year for shrublands, and varies slightly in savannas and croplands (Fig. 13). Note these values could not be interpreted as long-term trends because the time period we investigated does not extend into a decadal scale. The interannual variations are largest in shrublands according to the coefficient of variation (cv = standard deviation/mean) which is 35%, 19%, 40%, 33% and 21% in forests, savannas, shrublands, grasslands, and croplands, separately.

Annual burned area also varies considerably at state levels. The coefficient of variation is larger than 60% in half the states (Fig. 14). It is over 90% in Colorado, and Oregon, while it is less than 30% in Texas, Oklahoma, Arkansas, and Missouri. Because of the short time period (seven years) of data used in this study, the temporal trend in the burned area is generally not significant at 0.05 confident levels.

5. Discussion and conclusions

This study has, for the first time, developed an algorithm to simulate the burned areas at high temporal and spatial resolution from active GOES fire data. It demonstrates that the burned areas are equivalent to half-hourly fire sizes simulated using the diurnal patterns. Evaluation and validation reveal that the burned areas simulated from GOES fire data account for more than 82% of the variation in both the ETM+-based burn scars in individual fire events and the national fire inventory data in the matched grid cells. Apparently, this algorithm is robust to reconstruct diurnal burned areas, especially for the large fire events.

Spatially, large burned areas are dominated in the western CONUS while small values are densely distributed along the central and lower Mississippi Valley. Diurnal pattern of biomass burning during the seven years presents local peak burning time varying around 11:00–14:00 across CONUS. The pattern is most distinctive in agricultural regions because of the impact of human activities and it is relatively weak in forests where fires generally last for several days. Seasonal variability in burned area is also remarkable. Biomass burning generally occurs during summer, which causes more than 56% of annual burned areas. Contrary to the consistent patterns in diurnal and seasonal variations, interannual burned areas vary greatly. The annual burned areas change with a variation coefficient of 20%–40% in different ecosystems and larger than 90% in some states during past seven years. This interannual variation in burned areas is likely associated with recent climate change and effective fire suppressions (Schoennagel et al., 2004). The warming climates and fuel accumulations can induce the increase of burned areas while the fire suppressions and fuel reductions decrease the burned areas. However, large forest fires are mainly influenced by climate changes (Schoennagel et al., 2004).

This algorithm, unlike previous efforts that estimate burned areas by clustering active fire counts for a large grid cell (e.g., 0.5°) and a long time period (e.g., monthly), processes each GOES fire pixel individually and simulates burned areas every half hour. This product has a potential to contribute to the improvement of the understanding of greenhouse gases and aerosols released from wildland fires at various temporal scales. Particularly, because the burned area is retrieved from active fire hotspots, this algorithm makes it feasible to estimate emissions of biomass burning in near real time. This is critical for air quality forecasting which requires high temporal frequency of biomass burning emissions in near real time.

Finally, it is important to note that this algorithm currently has some limitations. The accuracy of the simulated burned area is strongly dependent on the quality of GOES fire size data. Burned area can not be provided for small fires where fire events are not detected by GOES imager at all. The geo-location in current GOES fires contains biases which have strong impacts on the estimates of diurnal patterns of fire sizes for individual GOES pixels. Moreover, the conversion coefficient between fire size and burned area may vary with the temporal resolution of fire detections. Therefore, further validation is desired before the widely use of this burned area data, particularly, the diurnal variation in burned areas. Finally, fire data quality is expected to be improved with NOAA's next generation geostationary satellite (GOES-R) which observes CONUS every 5 min with a spatial resolution of 2 km (Schmit et al., 2005), and will improve the estimates of the related burned area greatly.

Acknowledgments

We wish to thank Christopher Schmidt and Elaine Prins for providing GOES WF_ABBA fire data, Mark Ruminski for suggestions, Chuanyu Xu for preparing some figures, and four anonymous reviewers for constructive comments. The views, opinions, and findings contained in these works are these of the author(s) and should not be interpreted as an official NOAA or US Government position, policy, or decision.

References

Andreae, M. O., & Merlet, P. (2001). Emission of trace gasses and aerosols from biomass burning. *Global Biogeochemical Cycles*, *15*(4), 955–966.

Beck, J. A., Alexander, M. E., Harvey, S. D., & Beaver, A. K. (2001). Forecasting diurnal variation in fire intensity for use in wildland fire management applications. *Fourth Symposium on Fire and Forest Meteorology Meeting, 13–15 November 2001, Reno Nevada, USA*.

Boschetti, L., Brivio, P. A., Eva, H. D., Gallego, J., Baraldi, A., & Gregoire, J. M. (2006). A sampling method for the retrospective validation of global burned area products. *IEEE-Transactions on Geoscience and Remote Sensing*, *44*, 1765–1773.

Boschetti, L., Eva, H. D., Brivio, P. A., & Grégoire, J. M. (2004). Lessons to be learned from the comparison of three satellite-derived biomass burning products. *Geophysical Research Letters*, *31*(L21501). doi:10.1029/2004GL021229.

Briggs, W. L., & Hensen, V. E. (1995). *The DFT: An Owner's Manual for the Discrete Fourier Transform.* Philadelphia: Society for Industrial and Applied Mathematic.

Brown, J. F., Loveland, T. R., Ohlen, D. O., & Zhu, Z. (1999). The global land-cover characteristics database: The users' perspective. *Photogrammetric Engineering and Remote Sensing*, *65*, 1,069–1,074.

Cahoon, D. R., Stocks, B. J., Alexander, M. E., Baum, B. A., & Goldammer, J. G. (2000). Wildland fire detection from space: Theory and application. In J. L. Innes, M. M. Verstraete, & M. Beniston (Eds.), *Biomass Burning and its Inter-Relationships with the Climate System* (pp. 151–169). Boston: Kluwer Academic.

Chidumayo, E. N. (1987). A shifting cultivation land use system under population pressure in Zambia. *Agroforestry Systems*, *5*, 15–25.

Cochrane, M. A. (2003). Fire science for rainforests. *Nature*, *421*, 913–919.

Conard, S., Sukhinin, A., Stocks, B., Cahoon, D., Davidenko, E., & Ivanova, G. (2002). Determining effects of area burned and fire severity on carbon cycling and emissions in Siberia. *Climatic Change*, *55*, 197–211.

Countryman, C. M. (1966). The concept of fire environment. *Fire Control Notes*, *27*, 8–10.

Dozier, J. (1981). A method for satellite identification of surface temperature fields of subpixel resolution. *Remote Sensing of Environment*, *11*, 221–229.

Duncan, B. N., Martin, R. V., Staudt, A. C., Yevich, R., & Logan, J. A. (2003). Interannual and seasonal variability of biomass burning emissions constrained by satellite observations. *Journal of Geophysical Research*, *108*(D2), 4100. doi:10.1029/2002JD002378.

EPA (2003). *Documentation for the Draft 1999 National Emissions Inventory (Version 3.0) for Criteria Air Pollutants and Ammonia (Area Sources).* Research Triangle Park, NC, USA: E.H. Pechan & Asso. Inc. Office of Air Quality Planning and Standards.

Epting, J., Verbyla, D., & Sorbel, B. (2005). Evaluation of remotely sensed indices for assessing burn severity in interior Alaska using Landsat TM and ETM+. *Remote Sensing of Environment*, *96*, 328–339.

Eva, H., & Lambin, E. F. (1998). Remote sensing of biomass burning in tropical regions: Sampling issues and multisensor approach. *Remote Sensing of Environment*, *64*, 292–315.

Finn, M. (2001). British Columbia Forest Service adds new software for wildland firefighting. *Fire Management Today*, *61*(2), 43–44.

Fraser, R. H., & Li, Z. (2002). Estimating fire-related parameters in boreal forest using SPOT VEGETATION. *Remote Sensing of Environment*, *82*, 95–110.

French, N. H. F., Goovaerts, P., & Kasischke, E. S. (2004). Uncertainty in estimating carbon emissions from boreal forests fires. *Journal of Geophysical Research*, *109*(D14S08). doi:10.1029/2003JD003635.

Giglio, L. (2007). Characterization of the tropical diurnal fire cycle using VIRS and MODIS observations. *Remote Sensing of Environment*, *108*, 407–421.

Giglio, L., & Kendall, J. D. (2001). Application of the Dozier retrieval to wildfire characterization — A sensitivity analysis. *Remote Sensing of Environment*, *77*, 34–49.

Giglio, L., Kendall, J. D., & Mack, R. (2003). A multi-year active dataset for the tropics derived from the TRMM VIRS. *International Journal of Remote Sensing*, *24*, 4505–4525.

Giglio, L., van der Werf, G. R., Randerson, J. T., Collatz, G. J., & Kasibhatla, P. (2006). Global estimation of burned area using MODIS active fire observations. *Atmospheric Chemistry and Physics*, *6*, 957–974.

Ichoku, C., & Kaufman, Y. J. (2005). A method to derive smoke emission rates from MODIS fire radiative energy measurements. *IEEE Transactions on Geoscience and Remote Sensing*, *43*(11), 2636–2649.

Ito, A., & Penner, J. E. (2004). Global estimates of biomass burning emissions based on satellite imagery for the year 2000. *Journal of Geophysical Research*, *109*(D14S05). doi:10.1029/2003JD004423.

Justice, C. O., Giglio, L., Korontzi, S., Owens, J., Morisette, J. T., Roy, D., Descloitres, J., Alleaume, S., Petitcolin, F., & Kaufman, Y. (2002). The MODIS fire products. *Remote Sensing of Environment*, *83*, 244–262.

Kasischke, E. S., Hewson, J. H., Stocks, B., van der Werf, G. R., & Randerson, J. T. (2003). The use of ATSR active fire counts for estimating relative patterns of biomass burning — A study from the boreal forest region. *Geographical Research Letter*, *30* (18), 1969. doi:10.1029/2003GL017859.

Key, C. H. (2006). Ecological and sampling constraints on defining landscape fire severity. *Fire Ecology*, *2*(2), 34–59.

Key, C. H., & Benson, N. C. (1999). Measuring and remote sensing of burn severity. In L.F. Neuenschwander and K. C. Ryan (Eds.), Proceedings Joint Fire Science Conference andWorkshop, Vol. II, Boise, ID, 15–17 June 1999. University of Idaho and International Association of Wildland Fire. 284 pp.

Korontzi, S., McCarty, J., Loboda, T., Kumar, S., & Justice, C. (2006). Global distribution of agricultural fires in croplands from 3 years of Moderate Resolution Imaging Spectroradiometer (MODIS) data. *Global Biogeochemical Cycles*, *20*(GB2021). doi:10.1029/2005GB002529.

Leenhouts, B. (1998). Assessment of biomass burning in the coterminous United States. *Conservation Ecology*, *2*(1), 1–24.

Li, Z., Nadon, S., Cihlar, J., & Stocks, B. (2000). Satellite-based mapping of Canadian boreal forests: Evaluation and comparison of algorithms. *International Journal of Remote Sensing*, *21*(16), 3071–3082.

Loboda, T. V., & Csiszar, I. A. (2007). Reconstruction of fire spread within wildland fire events in Northern Eurasia from the MODIS active fire product. *Global And Planetary Change*, *56*, 258–273.

Lü, A., Tian, H., Liu, M., Liu, J., & Melillo, J. M. (2006). Spatial and temporal patterns of carbon emissions from forests in China from 1950 to 2000. *Journal of Geophysical Research*, *111*(D05313). doi:10.1029/2005JD006198.

Malingreau, J. P. (1990). The contribution of remote sensing to the global monitoring of fires in tropical and subtropical ecosystems. In J. G. Goldammer (Ed.), *Fire in the Tropical Biota, Ecosystem Processes and Global Challenges* (pp. 337–369). Berlin: Springer-Verlag.

McRae, D. J., Jin, J. Z., Conard, S. G., Sukhinin, A. I., Ivanova, G. A., & Blake, T. W. (2005). Infrared characterization of fine-scale variability in behavior of boreal forest fires. *Canadian Journal of Forest Research-Revue Canadienne De Recherche Forestiere*, *35* (9), 2194–2206.

Pereira, J. M., Pereira, B. S., Barbosa, P., Stroppiana, D., Vasconcelos, M. J. P., & Grégoire, J. M. (1999). Satellite monitoring of fire in the EXPRESSO study area during the 1996 dry season experiment: Active fires, burnt area, and atmospheric emissions. *Journal of Geophysical Research-Atmosphere*, *104*(D23), 30701–30712.

Prins, E. M., & Menzel, W. P. (1992). Geostationary satellite detection of biomass burning in South America. *International Journal of Remote Sensing*, *13*, 2783–2799.

Prins, E. M., & Menzel, W. P. (1994). Trends in South American biomass burning detected with the GOES visible infrared spin scan radiometer atmospheric sounder from 1983 to 1991. *Journal of Geophysical Research*, *99*(D8), 16719–16735.

Prins, E. M., Feltz, J. M., Menzel, W. P., & Ward, D. E. (1998). An overview of GOES-8 diurnal fire and smoke results for SCAR-B and 1995 fire season in South America. *Journal of Geophysical Research*, *103*(D24), 31821–31835.

Pu, R., Li, Z., Gong, P., Csiszar, I., Fraser, R., Hao, W., Kondragunta, S., & Weng, F. (2007). Development and analysis of a 12-year daily 1-km forest fire dataset across North America from NOAA/AVHRR data. *Remote Sensing of Environment*, *108*, 198–208.

Reid, J. S., Prins, E. M., Westphal, D. L., Schmidt, C. C., Richardson, K. A., Christopher, S. A., et al. (2004). Real-time monitoring of South American smoke particle emissions and transport using a coupled remote sensing/box-model approach. *Geophysical Research Letter*, *31*(L06107). doi:10.1029/2003GL018845.

Roberts, G., Wooster, M. J., Perry, G. L., Drake, N., Rebelo, L. M., & Dipotso, F. (2005). Retrieval of biomass combustion rates and totals from fire radiative power observations: Application to southern Africa using geostationary SEVIRI imagery. *Journal of Geophysical Research*, *110*(D21111). doi:10.1029/2005JD006018.

Robinson, J. M. (1991). Fire from space: Global fire evaluation using infrared remote sensing. *International Journal of Remote Sensing*, *12*, 3–24.

Rothermel, R. C., & Mutch, R. W. (1986). Behavior of the life-threatening Butte Fire: August 27–29, 1985. *Fire Manage Notes*, *47*(2), 14–24.

Roy, D. P., Boschetti, L., & Trigg, S. N. (2006). Remote sensing of fire severity: Assessing the performance of the normalized burn ratio. *IEEE Geoscience and Remote Sensing Letters*, *3*. doi:10.1109/LGRS.2005.858485.

Roy, D. P., Lewis, P. E., & Justice, C. O. (2002). Burned area mapping using multi-temporal moderate spatial resolution data — A bi-directional reflectance model-based expectation approach. *Remote Sensing of Environment*, *83*, 263–286.

Schmidt, C. C., & Prins, E. M. (2003). GOES wildfire ABBA applications in the western hemisphere. *Second International Wildland Fire Ecology and Fire Management Congress and Fifth Symposium on Fire and Forest Meteorology, 16–20 November, Orlando, Florida.*

Schmit, T. J., Gunshor, M. M., Menzel, W. P., Gurka, J. J., Li, J., & Bachmeier, A. S. (2005). Introducing the next-generation advanced baseline imager on GOES-R. *Bulletin of the American Meteorological Society*, *86*, 1079–1096.

Schoennagel, T., Veblen, T. T., & Romme, W. H. (2004). The interaction of fire, fuels, and climate across Rocky Mountain forests. *BioScience*, *54*(7), 661–676.

Scholes, R. J., Kendall, J. D., & Justice, C. O. (1996). The quantity of biomass burned in southern Africa. *Journal of Geophysical Research-Atmosphere*, *101*, 23667–23676.

Schreiner, A. J., Schmit, T. J., & Menzel, W. P. (2001). Observations and trends of clouds based on GOES sounder data. *Journal of Geophysical Research*, *106*(D17), 20,349–20,363.

Schroeder, M. J., & Buck, C. C. (1970). *Fire weather — a guide for application of meteorological information to forest fire control operations. Agricture Handbook 360.* Washington, DC: U.S. Department Agriculture 229pp.

Simon, M., Plummer, S., Fierens, F., Hoelzemann, J. J., & Arino, O. (2004). Burnt area detection at global scale using ATSR-2: The GLOBSCAR products and their qualification. *Journal of Geophysical Researsh-Atmosphere*, *109*(D14S02). doi:10.1029/2003JD003622.

Soja, A. J., Al-Saadi, J., Pierce, B., Kittaka, C., Szykman, J., Giglio, L., et al. (2007). A methodology for estimating area burned using satellite-based data in near-real-time in Oregon and Arizona. *16th Annual International Emission Inventory Conference Emission Inventories: "Integration, Analysis, and Communications", Raleigh, May 14–17, 2007.*

Soja, A. J., Sukhinin, A. I., Cahoon, D. R., Shugart, H. H., & Stackhouse, P. W. (2004). AVHRR-derived fire frequency, distribution and area burned in Siberia. *International Journal of Remote Sensing*, *25*, 1939–1960.

Tansey, K., Grégoire, J. M., Stroppiana, D., Sousa, A., Silva, J., Pereira, J. M. C., et al. (2004). Vegetation burning in the year 2000: Global burned area estimates from SPOT VEGETATION data. *Journal of Geophysical Research-Atmosphere*, *109*(D14S03). doi:10.1029/2003JD003598.

Van Wagtendonk, J. W., Root, R. R., & Key, C. H. (2004). Comparison of AVIRIS and Landsat ETM+ detection capabilities for burn severity. *Remote Sensing of Environment*, *92*, 397–408.

Weaver, J. F., Lindsey, D., Bikos, D., Schmidt, C. C., & Prins, E. (2004). Fire detection using GOES rapid scan imagery. *Weather and Forecasting*, *19*, 496–510.

Wiedinmyer, C., Quayle, B., Geron, C., Belote, A., McKenzie, D., Zhang, X., et al. (2006). Estimating emissions from fires in North America for air quality modeling. *Atmospheric Environment*, *40*, 3419–3432.

WRAP (2005a). *Inter-RPO National 2002 Wildfire Emissions Inventory-Final Work Plan.*: Air Sciences & EC/R Project No. 178-7.

WRAP (2005b). *2002 Fire emission inventory for the WRAP region — phase II.*: Air Sciences, Inc. Project No. 178, July 22, 2005. Available at http://strait.cfr.washington.edu/~smo/share/2002%20Phase%20II%20Fire%20EI/

Zhang, Y. H., Wooster, M. J., Tutubalina, O., & Perry, G. L. W. (2003). Monthly burned area and forest fire carbon emission estimates for the Russian Federation from SPOT VGT. *Remote Sensing of Environment*, *87*, 1–15.